VORTICAL FLOW SIMULATION USING AN UNSTRUCTURED-GRID EULER METHOD

P. Raj*, T.A. Kinard** and S.A. Vermeersch†
Lockheed Martin Aeronautical Systems
Marietta, GA 30063-0685, USA

Abstract

A computational fluid dynamics method for solving the Euler equations using unstructured tetrahedral grids is applied to simulate vortical flows on three configurations: delta wing, double-delta wing-body and wing-body-tail model. The principal objective is to assess the effectiveness of the method in predicting aerodynamic forces, moments and surface pressures up to maximum lift conditions at subsonic speeds. The primary assessment criteria are turnaround time and accuracy. The Euler method consists of a grid generation tool based on advancing front technique and a flow solver that uses an implicit cell-centered upwind algorithm. Solution sensitivity to grid density and flux limiter functions is investigated. Computed solutions are compared with the available experimental data and structured-grid Euler solutions. The results contribute to a better understanding of the capabilities and limitations of the method.

Introduction

Vortical flows are of special significance to aircraft designed for efficient supersonic cruise, such as advanced tactical fighters and high-speed civil transports. During take-off, landing, or maneuvering flight conditions, the flow invariably separates from the leading edges of their swept, slender wings resulting in the formation of vortices. In some instances, flow separation from the forebody produces additional vortices. These vortices strongly influence the aerodynamic characteristics whose accurate estimation is of critical importance to aircraft design. Forces and moments are needed to evaluate performance and handling qualities; surface pressures and flow-field data provide inputs for structural design as well as for propulsion-system and weapon-system integration.

To date, costly and time-consuming wind-tunnel tests have been used almost exclusively to produce the desired aerodynamic data to support design needs. A judicious mix of wind tunnels and computational fluid dynamics (CFD) affords a more cost-effective alternative. Successful pursuit of this alternative is predicated upon the availability of computational methods that provide rapid turnaround and reliable accuracy at low cost. Although past research has produced a variety of computational tools, they are not yet fully effective in meeting the design needs.

Methods based on the linearized potential-flow formulations were developed during the 1970s. These methods rely either on the use of Polhamus suction analogy[1] with vortex-lattice techniques[2-3] or the use of off-surface singularities in panel codes to explicitly model free-vortex sheets[4] whose location and strength are iteratively determined. Vortices cannot naturally evolve as a part of the solution. Although these methods are fast and affordable, they are unable to provide an accurate representation of the vortex itself and the associated flow field. Also, their predictions are less than reliable for transonic conditions as well as for flows with multiple interacting vortices or vortex burst.

During the 1980s, dramatic progress was made in methods to solve the Euler and Reynolds-averaged Navier-Stokes (RANS) equations using structured hexahedral grids. Euler methods are found to be quite capable of automatically capturing principal features of vortical flows, including vortex burst, for sharp-edged planforms.[5-7] This capability is directly attributable to the presence of artificial viscosity, whether explicitly added as in central-difference schemes or inherently present as in upwind schemes. Although the magnitude of artificial vicosity is small, it is sufficient to mimic the role of true viscosity in causing flow separation at the sharp edges. Secondary vortices arising from boundary-layer separation as well as primary vortices resulting from flow separation on smooth surfaces, e.g., round leading edges, may be simulated by coupling Euler methods with boundary-layer codes. However, the use of RANS methods is much more common.

Although impressive RANS solutions have been obtained,[7-9] some accuracy issues remain unresolved. For example, most RANS solutions use the thin-layer approximation with grids clustered near the solid surfaces; grids in the vortical-flow regions remain relatively coarse. Also, only second or third order accurate schemes have been employed. A recent study by Dacles-Mariani et al.[10] recommends using a minimum of 15-20 points across the vortex cores with a grid cell aspect ratio of 1. The study also suggests using higher-order accurate discretization, e.g., fifth order, to reduce numerical dissipation effects.

In spite of the substantially enhanced capabilities that structured-grid Euler and RANS methods offer, their effectiveness in the design process is severely hampered by long turnaround times associated with their application. The more widely-used methods employ either patched multiblock or overset hexahedral grids. Constructing such grids for complex geometries continues to be a time-consuming and labor-intensive task. The unstructured-grid CFD methods offer an attractive alternative and promise to significantly

---

* Technical Fellow, Computational Fluid Dynamics

** Senior Engineer, Aerodynamics Department

† Engineer, Aerodynamics Department

reduce turnaround time—from several weeks to a matter of days or hours—through more "automated" grid generation. Ongoing efforts are directed at both tetrahedral[11,12] and Cartesian/prismatic[13,14] grid methods.

The principal objective of the present study is to assess the effectiveness of a tetrahedral-grid Euler method for vortical flow simulation. The primary criteria are turnaround time and accuracy. The approach involves correlating computational solutions with the available experimental data as well as structured-grid Euler solutions for three test cases: (1) 74° delta wing (Figure 1); (2) 75°/62° double-delta wing-body (Figure 2); and (3) centerline tail modular transonic vortex interaction (MTVI) model (Figure 3). Solution sensitivity to flux limiter functions is also evaluated for the first two cases, and sensitivity to grid density is assessed for all three. Solutions are generated for a range of angle of attack (α) up to maximum lift. For the MTVI model, results for three sideslip angles (β) for a fixed α are also presented.

The remainder of the paper is divided into three sections. A brief overview of the method is presented first. This is followed by a discussion of results. A few concluding remarks complete the paper.

Unstructured-Grid Method

The unstructured-grid method[12] consists of three software packages that are sequentially executed: (1) GridTool/VGRID for geometry modeling and grid generation, (2) USM3D for flow solution, and (3) VPLOT3D for postprocessing. Only the basic features of these tools are highlighted in this section. Appropriate references are cited for readers interested in more details.

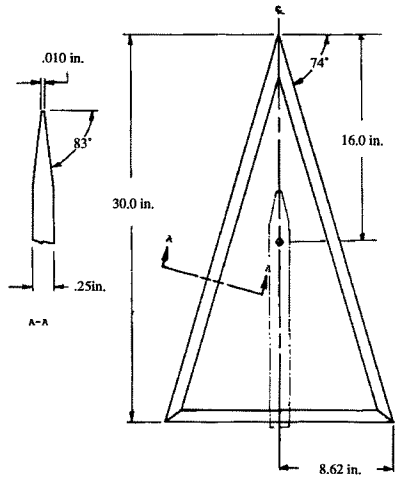

FIGURE 1 - 74° Delta Wing

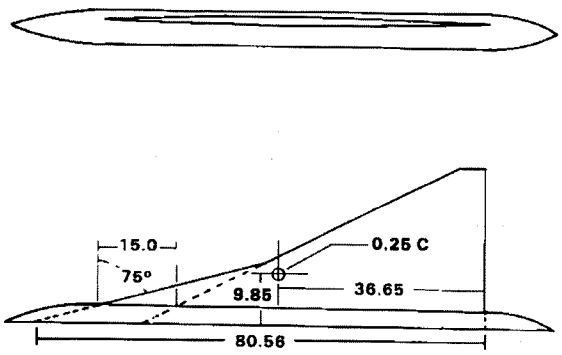

FIGURE 2 - 75°/62° Double Delta Wing Body

Grid Generation

The grid generation process starts with the GridTool[15] program reading in the configuration geometry file containing either a set of discrete points or data in IGES[16] format. A user interactively constructs curves and patches on the configuration surface, and sets up the far-field boundaries usually as a simple box to define a computational domain. Point and line sources are then prescribed to control the distribution of points on the bounding surfaces and in the interior. The output of GridTool is an input file for the VGRID code[17] used to generate the surface and volume grids.

The VGRID program, based on the advancing front method, uses a structured background mesh[18] to control the point distribution for both surface and volume grids. The background mesh is constructed by subdividing the entire flow domain into cells. Spacing information needed to control point distribution is stored at the nodes of the cells. Once the background mesh is created, the edges of the user-defined patches are subdivided into a desired number of points. The discretized edges define the initial front to triangulate the entire patch. After each patch is triangulated, the surface grid quality is checked automatically and any regions of poor quality are displayed. The user has the ability to modify the patches in order to achieve a better grid if necessary.

The triangulated patches form the initial front for the volume grid. The front is advanced into the field by introducing new points and forming tetrahedra. The code continues to run until either the domain is filled or no more tetrahedra can be formed thus leaving pockets or voids. These pockets are usually filled by removing a layer of tetrahedra around the pocket creating a larger void and a new front. The grid generator is restarted and new points are added until the grid is completed. A grid quality check is then initiated and tetrahedra with negative volumes and/or high skewness are identified. A few tetrahedra are removed from

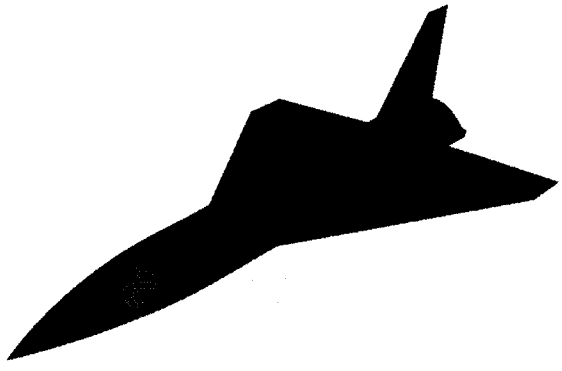

FIGURE 3 - Centerline Tail MTVI Model

the region of poor-quality grids and the region is refilled. Sometimes the background mesh has to be modified in order to generate an acceptable grid.

Flow Solution

The USM3D[19] flow solver uses a cell-centered finite-volume formulation to solve the time-dependent compressible-flow Euler equations for an ideal gas. Convective fluxes are computed using the well-known Roe's flux-difference or Van Leer's flux-vector splitting. Higher-order accuracy is achieved by reconstructing a multidimensional piecewise linear solution of the cell-averaged data which produces nonoscillatory solutions without using any flux limiter functions. Version 4.3[20] used here offers two options for flux limiter, minmod or superbee. Solution sensitivity to these options is investigated in this study.

The solution is advanced in time by either a 3-stage time-stepping scheme (combined with local time stepping and implicit residual smoothing as convergence acceleration mechanisms) or an implicit linearized backward Euler scheme. The code uses 45 words of core memory per cell and 14.5 μsec/cell/cycle for the explicit scheme, and 180 words per cell and 29 μsec/cell/cycle for the implicit scheme. The computer times are for a single-processor Cray C-90 run. The implicit scheme converges to a steady state in much less computer time,[21] by as much as a factor of 6, compared to the explicit scheme because a much larger time step can be used.

Two strategies are employed to enhance robustness. First, the time-marching process starts with a first-order accurate scheme and automatically switches to second-order accuracy after one order of magnitude reduction in average residual. Second, the Courant-Friedrichs-Lewy (CFL) number incrementally ramps up from an initial low value to a final high value, both specified by the user, over a prescribed number of cycles.

Postprocessing

VPLOT3D[12,17] is an interactive, graphical menu-driven program for extraction and display of the desired on- and off-body flow quantities as line or filled contours, vectors or particle traces. A user can also use it to visually examine regions of poor-quality grids and different boundary conditions. The ACE/gr[22] software package was used to produce x-y type plots.

Results and Discussion

Results for three test cases are presented in this section. Unless otherwise noted, all USM3D analyses were performed with an initial CFL number of 25 that ramped up to a final value of 75 over 50 cycles. Convergence criteria included two-to-three orders of magnitude reduction in residual plus no variation in the first three significant digits of the integrated force and moment values. Uniform free-stream conditions were used to initialize the flow field. Also, all solutions correspond to the second-order accurate scheme.

74° Delta Wing

The geometric features of this test case[23] are shown in Figure 1. Only half of the configuration was analyzed. All edges were treated as sharp and the sting was not modeled. Fifty patches were used to model the wing, plane of symmetry and outer boundaries of the computational domain. Points were clustered near the leading and trailing edges as well as along a line approximating the footprint of the wing vortex. Portions of the upper-surface and plane-of-symmetry grids are shown in Figure 4.

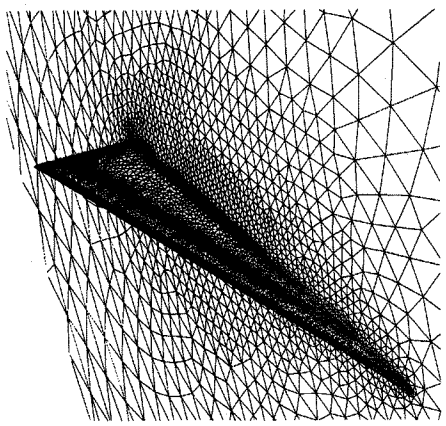

FIGURE 4 - A Perspective View of Grid About 74° Delta Wing

To evaluate solution sensitivity to grid density, solutions were obtained at 0.3 Mach number (M) and $\alpha = 20°$, on three grids: Grid 1 with 101413 cells, Grid 2 with 167086 cells, and Grid 3 with 226269 cells. No limiter function was used. The lift (C_L), drag (C_D) and pitching moment (C_M) coefficients are shown in Table 1. Computed C_p distributions are compared at four cross-plane stations in Figure 5. Note that X is the downstream distance from the apex, C_R is the root chord, and S(X) is local span. The solutions show relatively little sensitivity to grid density.

Table 1. Grid Sensitivity for Delta Wing

Grid	# Cells	CL	CD	CM
Grid 1	101413	0.8639	0.3104	–0.052
Grid 2	167086	0.8676	0.3116	–0.052
Grid 3	226269	0.8667	0.3112	–0.051

In Table 2, USM3D force and moment predictions using the minmod and superbee limiter functions are compared with the no-limiter results on Grid 2. The superbee and no-limiter results agree well, but they both differ from the minmod solution. The corresponding surface C_p distributions shown in Figure 6 also exhibit a similar behavior. Results for

Table 2. Flux Limiter Sensitivity for Delta Wing

Limiter	CL	CD	CM
Minmod	0.8075	0.2905	–0.047
None	0.8676	0.3116	–0.052
Superbee	0.8689	0.3116	–0.05

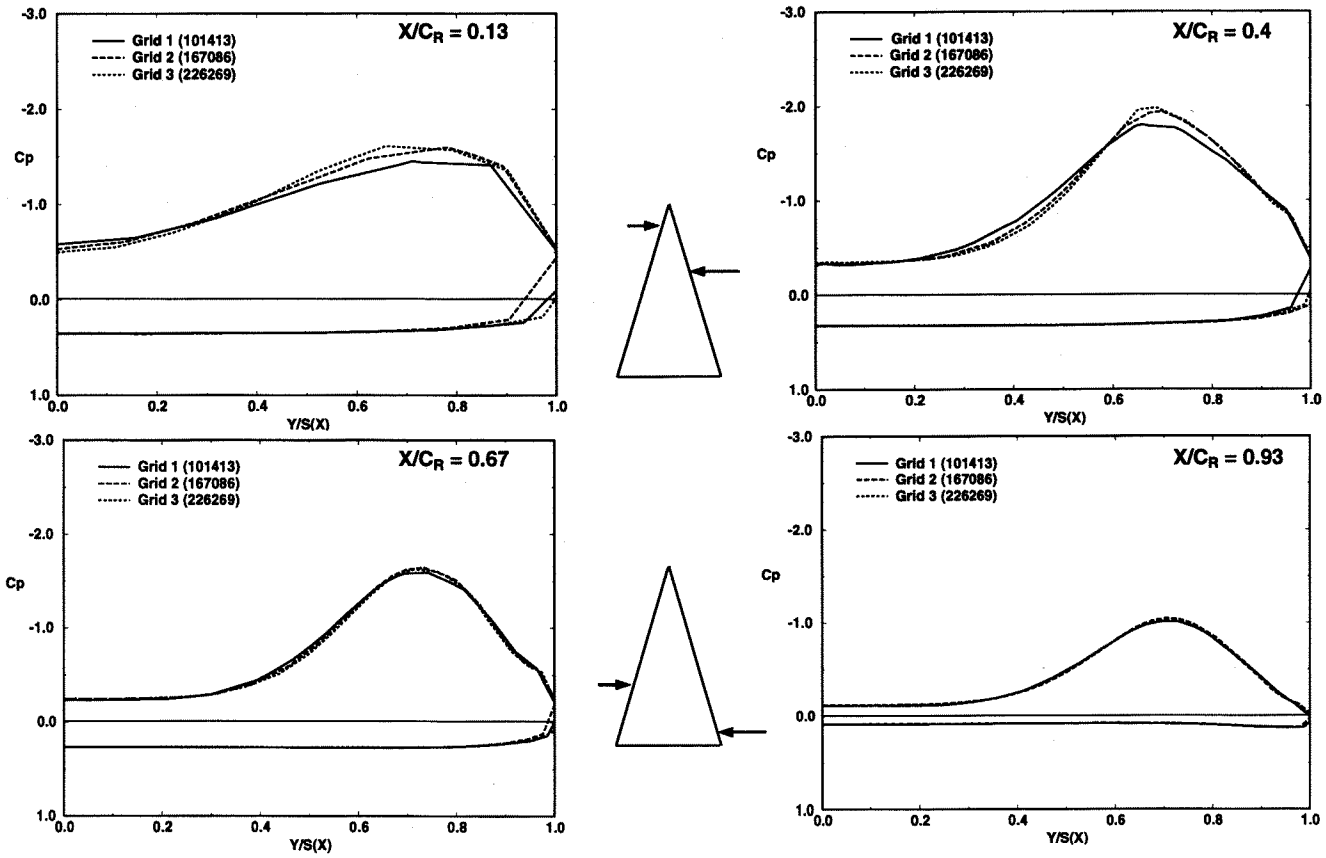

FIGURE 5 - Grid Sensitivity of Surface C_p in USM3D Analysis , 74° Delta Wing, M = 0.3, α = 20°

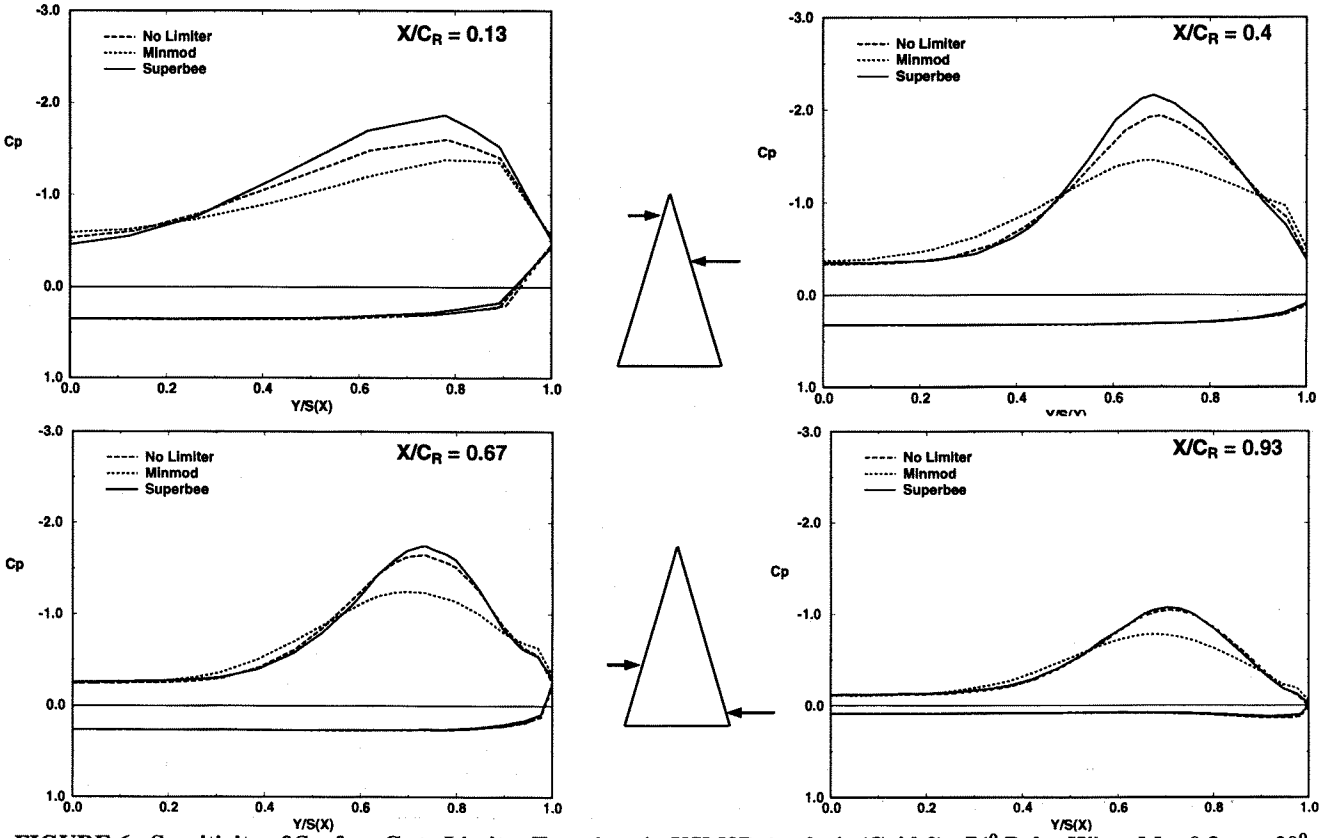

FIGURE 6 - Sensitivity of Surface C_p to Limiter Functions in USM3D Analysis (Grid 2) , 74° Delta Wing, M = 0.3, α = 20°

this case as well as others (not included here) on a cropped-delta wing and a double-delta wing-body show that superbee solutions are the least sensitive to grid density. Based on the sensitivity studies, Grid 2 and superbee limiter were used for all additional analyses of this test case.

Computed force and moment coefficients for twelve angles of attack are correlated with experimental data[23] in Figure 7. The general trends are captured up to $\alpha = 30^{\circ}$. All cases for $\alpha \leq 31^{\circ}$ were well converged in 400 cycles with forces and moments reaching a steady state after about 250 cycles. However, no converged solutions were obtained for $\alpha \geq 32^{\circ}$. Instead, the residual attained an oscillatory pattern and the forces and moments oscillated about a mean value as illustrated in Figure 8 by the convergence histories of average residual and lift coefficient for $\alpha = 35^{\circ}$. Here R is the current value and R1 is the initial value of the average residual. For the sake of comparison, the figure also includes the corresponding convergence histories for a converged solution at $\alpha = 15^{\circ}$. The oscillatory pattern is indicative of vortex instability or burst with the flow field being steady everywhere else except in localized regions. This behavior is consistent with that exhibited by structured-grid Euler solutions.[5] Since the present solution process is not time accurate, the unconverged solutions cannot be considered quantitatively accurate representations of the entire flow field. Note that the mean values are plotted in Figure 7 for $\alpha \geq 32^{\circ}$.

In Figure 9, the USM3D surface C_p distributions for the $\alpha = 20^{\circ}$ case are compared with structured-grid TEAM solutions and experimental data. The TEAM solutions were obtained using a grid with nearly 250000 cells. The two computed solutions are in fairly good agreement with each other except at the two most forward stations. Both solutions show discrepancies with experimental data which are largely due to viscous effects being not modeled in the computations.[7]

75°/62° Double-Delta Wing Body

The basic geometric features of this test case[24] are shown in Figure 2. Only half of the configuration was analyzed. All edges on the wing were treated as sharp. Twenty patches were used to model the configuration and the outer bounding surfaces. Points were clustered around the leading and trailing edges of the wing. Portions of the grids on the surface and the plane of symmetry are shown in Figure 10.

To evaluate solution sensitivity to grid density, solutions were obtained at $M = 0.3$, $\alpha = 20^{\circ}$, on three grids with 269319, 395073, and 473506 cells. The superbee limiter function was used. The solutions showed relatively little sensitivity to grid density. The coarsest grid with 269319 cells and superbee limiter were employed for all additional runs.

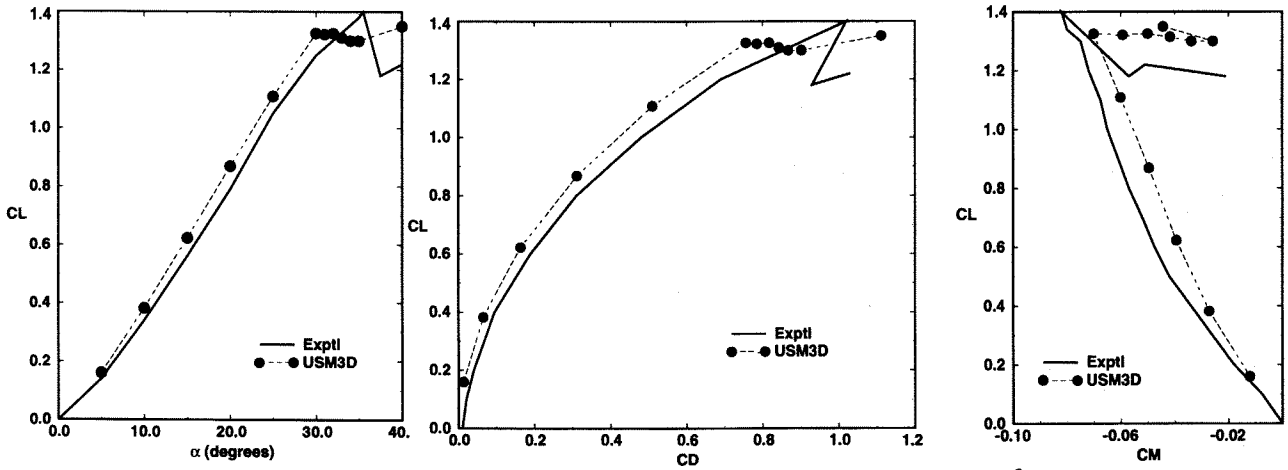

FIGURE 7 - Correlations of Computed and Measured Force and Moment Coefficients, 74° Delta Wing, M = 0.3

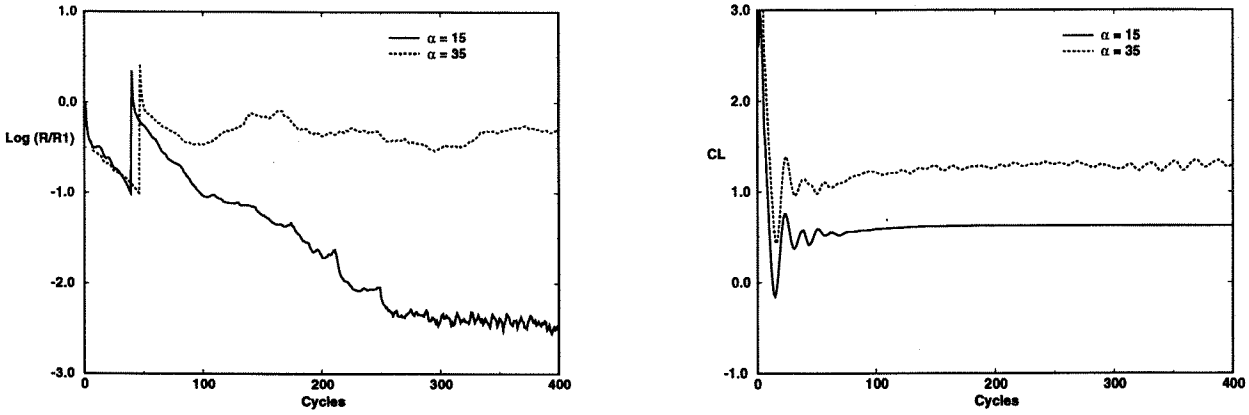

FIGURE 8 - Comparison of Convergence Histories for USM3D Analyses, 74° Delta Wing, M = 0.3, α = 15° and 35°

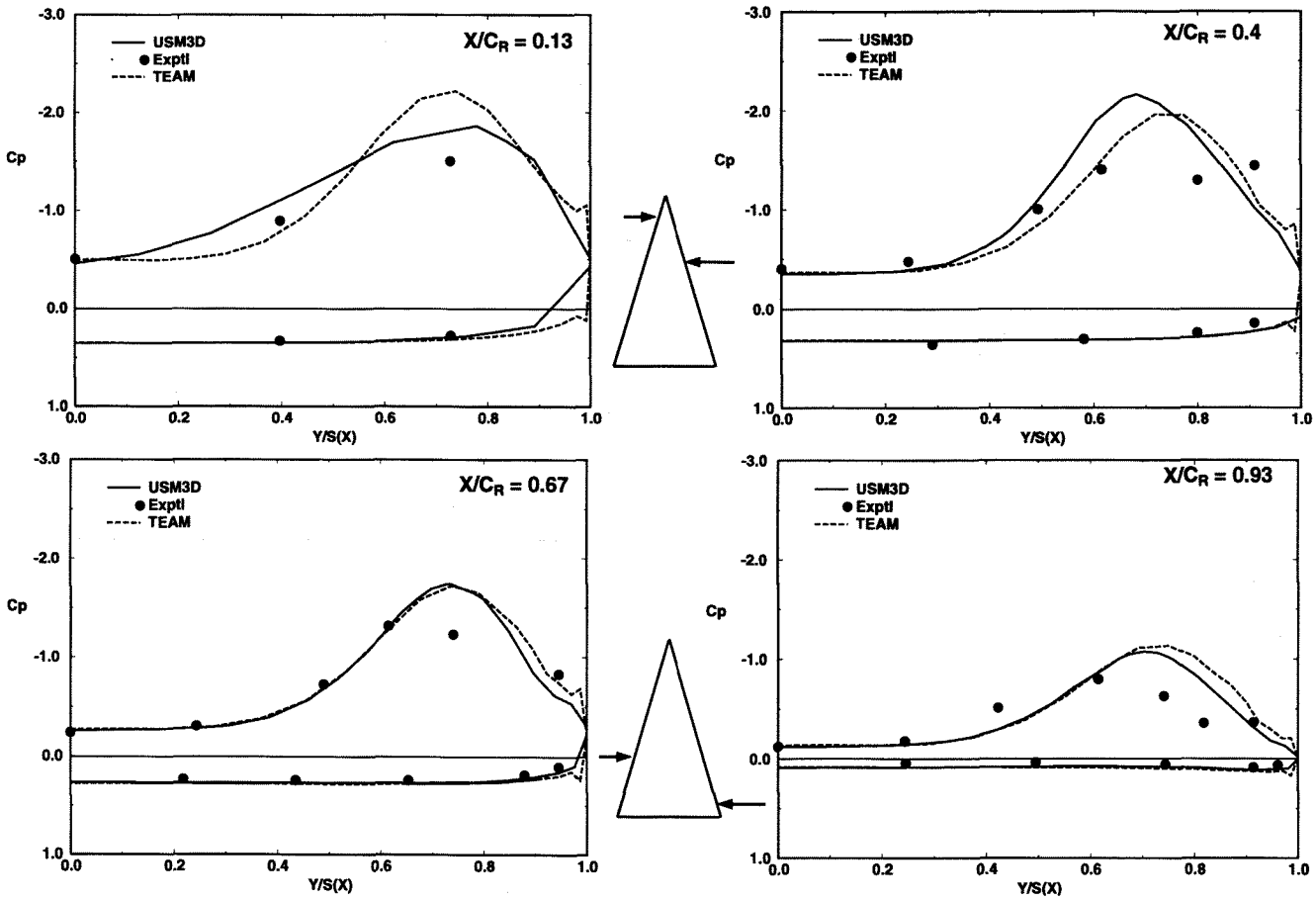

FIGURE 9 - Correlation of Computed and Measured Surface C_p, 74° Delta Wing, M = 0.3, α = 20°

Computed lift and drag coefficients for eight angles of attack are correlated with experimental data[24] in Figure 11. The general trends are captured up to $\alpha = 25°$. More than two orders of magnitude reduction in average residual was achieved in 400 cycles for α up to 15°; 600 and 800 cycles were required for α of 20° and 25° respectively. No converged solutions were obtained for $\alpha \geq 30°$. Much like the delta wing case, the average residual as well as forces and moments attained an oscillatory pattern indicating vortex instabilities or burst.

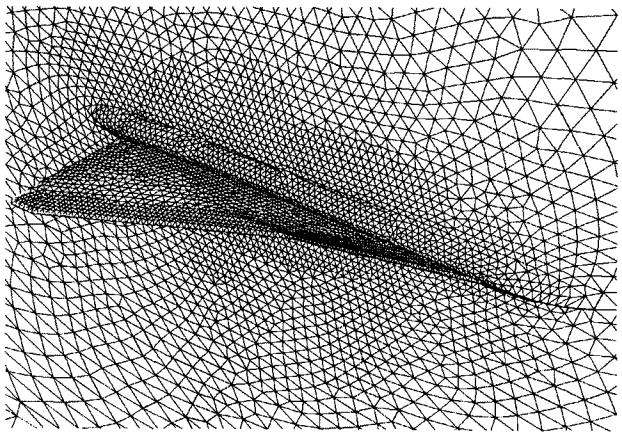

FIGURE 10 - A Perspective View of Grid About 75°/62° Double-Delta Wing-Body Configuration

The USM3D force and moment predictions agree well with those of the structured-grid TEAM computations[5] except that the TEAM solutions exhibited a lack of convergence for $\alpha \geq 25°$ whereas the USM3D code produced converged solutions for all angles of attack up to and including 25°. The discrepancy is most likely due to relatively large cells on the aft part of the wing in TEAM grid which had only 105633 nodes. Large cell sizes result in poor flow resolution as well as higher numerical dissipation. The related issues need to be further investigated.

For this case, surface C_p are correlated for α = 20° at three cross-plane stations shown in Figure 12. In Figure 13, the USM3D solutions are compared with TEAM solutions[5] on a grid with nearly 250000 cells and with experimental data. The two computed solutions are in fair agreement with each other except at the aftmost station where the higher peak in the USM3D solution suggests the presence of a stronger vortex. Both solutions show discrepancies with experimental data which are largely due to viscous effects being not modeled in the computations.

Centerline Tail MTVI Model

A perspective view of the surface geometry of the centerline tail MTVI model is shown in Figure 3. The chined forebody has an included angle of 30°. The wing has a cropped delta planform with a leading-edge sweep of 60° and an aspect ratio of 1.8. All edges were treated as sharp and the

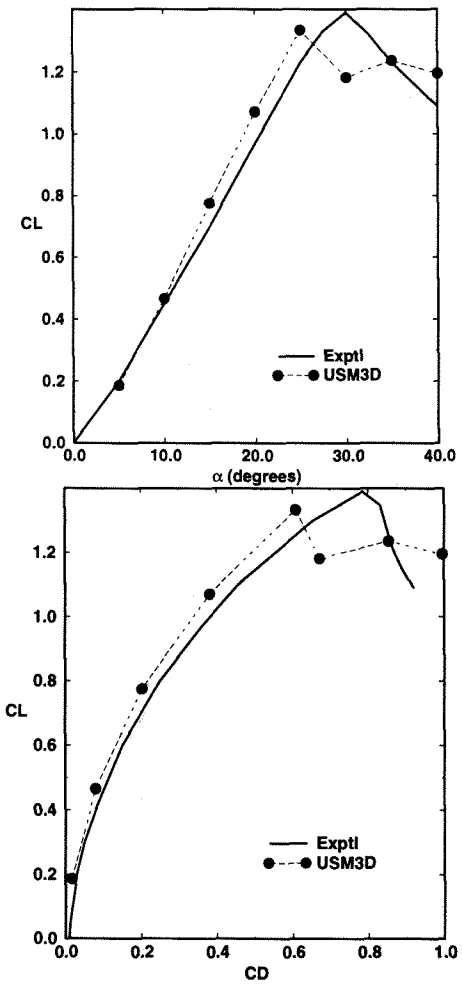

FIGURE 11 - Correlation of Computed and Measured Forces for 75°/62° Double Delta Wing Body, M = 0.3

sting was modeled. The entire surface was divided into 92 patches. Points were clustered near the perimeter of the wing and vertical tail, the chine, and a line approximating the footprint of the wing vortex. Portions of the upper-surface and plane-of-symmetry grid are shown in Figure 14. It took approximately 8 labor hours to build the grid which contrasts with about 64 hours required to build a structured grid for Euler analysis on a similar configuration.[7]

In order to select a "suitable" grid, a grid sensitivity study was conducted using four grids with 405815, 529425, 613826 and 714392 cells. Solutions were obtained at M = 0.4, $\alpha = 20^{\circ}$, and $\beta = 0^{\circ}$. Based upon a comparison of com-

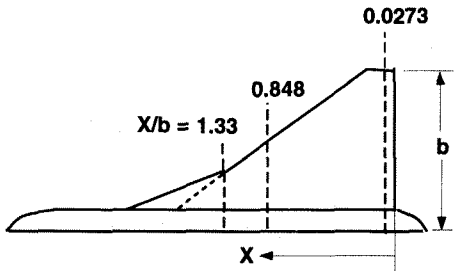

FIGURE 12 - Locations of Cross-plane Stations for C_p Correlations on 75°/62° Double-Delta Wing-Body

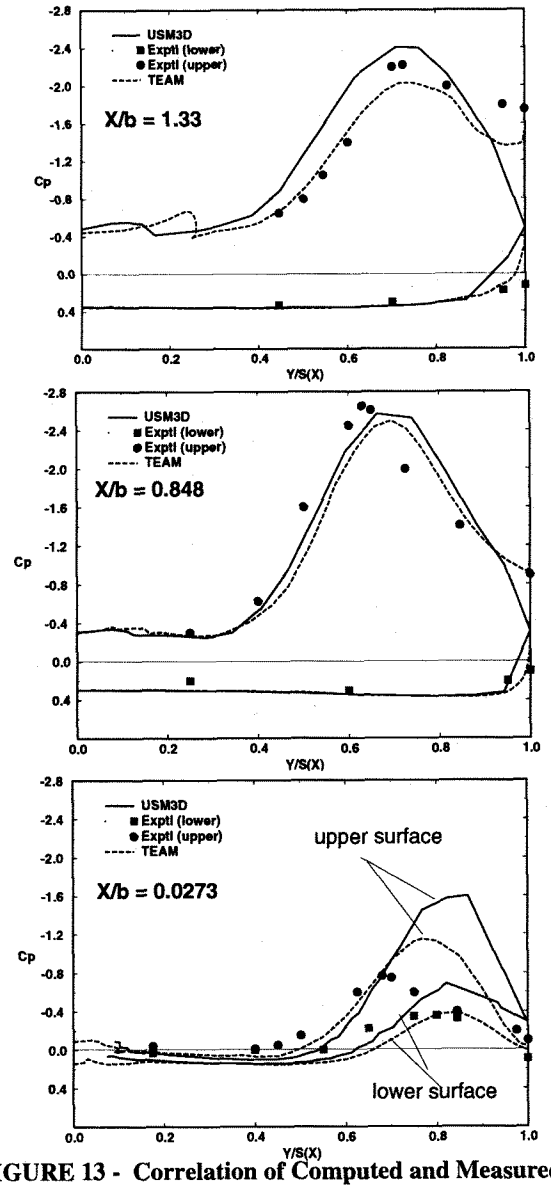

FIGURE 13 - Correlation of Computed and Measured Surface C_p Distributions for 75°/62° Double-Delta Wing-Body, M = 0.3, $\alpha = 20^{\circ}$

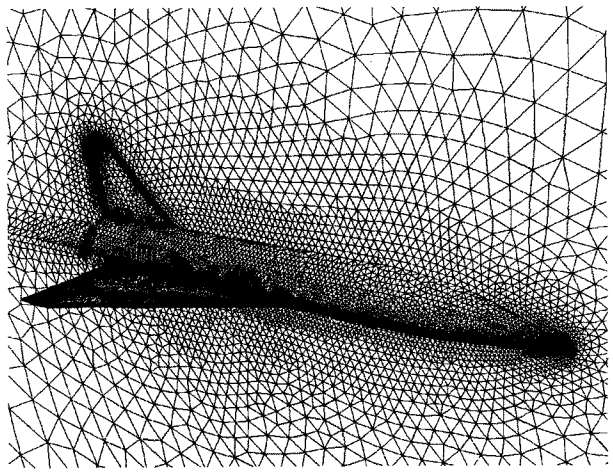

FIGURE 14 - A Perspective View of Grid About Centerline Tail MTVI Model

puted forces and moments as well as cross-plane surface pressures,[25] the grid with 613826 cells was selected for all symmetric-flow analyses. For asymmetric cases, the grid was reflected about the longitudinal plane of symmetry.

Computed force and moment coefficients for five angles of attack are correlated with experimental data[25] in Figure 15. The general trends are captured up to $\alpha = 25^\circ$. Converged solutions with more than three orders of magnitude reduction in average residual were obtained in 300 cycles. No converged solutions was obtained for $\alpha = 30^\circ$. Just like the other two test cases, the lack of convergence was caused by vortex instabilities or burst. The mean values of forces and moments are plotted in Figure 15 for $\alpha = 30^\circ$.

Computed pitching (C_m), rolling (C_r) and yawing (C_n) moment coefficients for $\beta = 2^\circ$, 4° and 7° with $\alpha = 25^\circ$ are correlated with experimental data in Figure 16. The solutions did not converge for any of these cases due to vortex instabilities; mean values are plotted in Figure 16. Note that converged solutions could be obtained[25] for the same three β values but at a lower α of 15°.

For surface C_p correlations, experimental data is available at six cross-plane stations shown in Figure 17.

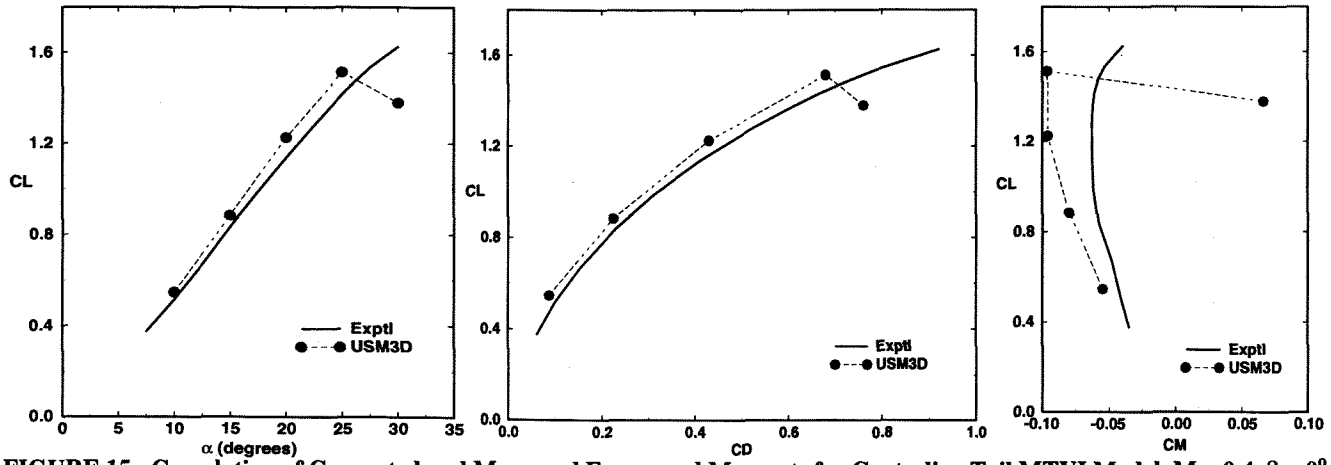

FIGURE 15 - Correlation of Computed and Measured Forces and Moments for Centerline Tail MTVI Model, M = 0.4, $\beta = 0^\circ$

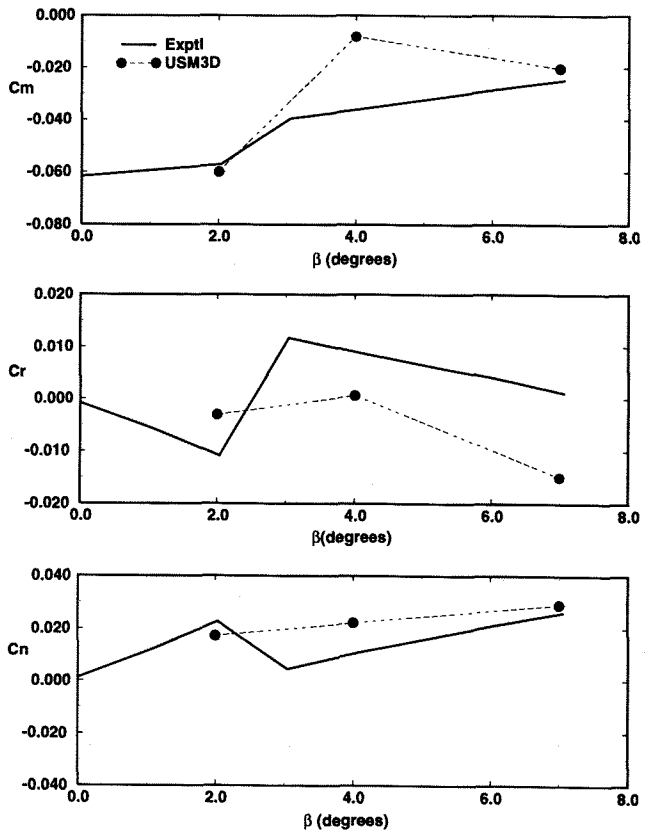

FIGURE 16 - Correlation of Computed and Measured Moments for Centerline Tail MTVI Model, M = 0.4, $\alpha = 25^\circ$ (Asymmetric Conditions)

Three stations are on the chined forebody section and the other three on the aftbody-wing section. The computed and measured surface C_p distributions at $\alpha = 25^\circ$, shown in Figure 18, are in fairly good agreement overall. However, the inviscid solutions fail to accurately model the effect of secondary vortices on the primary vortical features as indicated by the correlations at X = 10.45, 14.5 and 28.05 stations.

In Figure 19, the computed and measured surface C_p distributions are compared at four cross-plane stations for the $\alpha = 25^\circ$, $\beta = 4^\circ$, case. The USM3D solution exhibits relatively larger discrepancies with the experimental data on the upper surface of the model on the starboard side as compared to the port side. The effect of vortex instability can be seen in the experimetnal C_p distribution on the starboard side at the last two stations, X = 23.55 and 28.05, and in the USM3D solutions at the X = 28.05 station. Additional results for this case are presented in References 25 and 26.

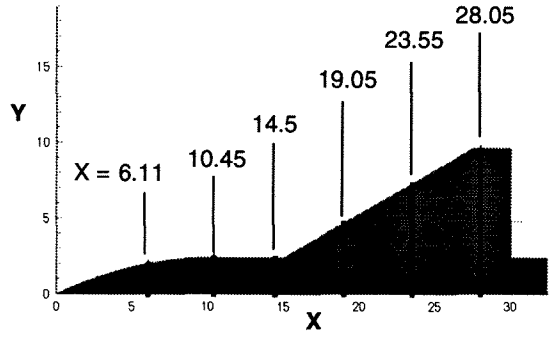

FIGURE 17 - Locations of MTVI Cross-plane Stations

Concluding Remarks

The results of computational simulations of vortical flows presented in this paper contribute to developing a better understanding of the capabilities and limitations of an unstructured tetrahedral-grid Euler method consisting of GridTool/VGRID codes for grid generation and the USM3D code for flow solution.

(1) Using the unstructured-grid method can result in a considerable reduction in the turnaround time as compared to the structured-grid methods with most of the benefit coming from faster grid generation. In this study, a reduction in turnaround time by a factor of 8 was achieved for the wing-body-tail MTVI model. The reduction may not be as sizable for simple geometries such as wing and wing-body, but it can be even more substantial for complex shapes like a full aircraft.

(2) The USM3D flow solver itself was found to be quite robust and capable of simulating vortical flows to levels of accuracy comparable to those of the structured-grid methods using grids with comparable number of cells. However, the required computer memory is substantially higher by as much as a factor of 4.5. Means of reducing

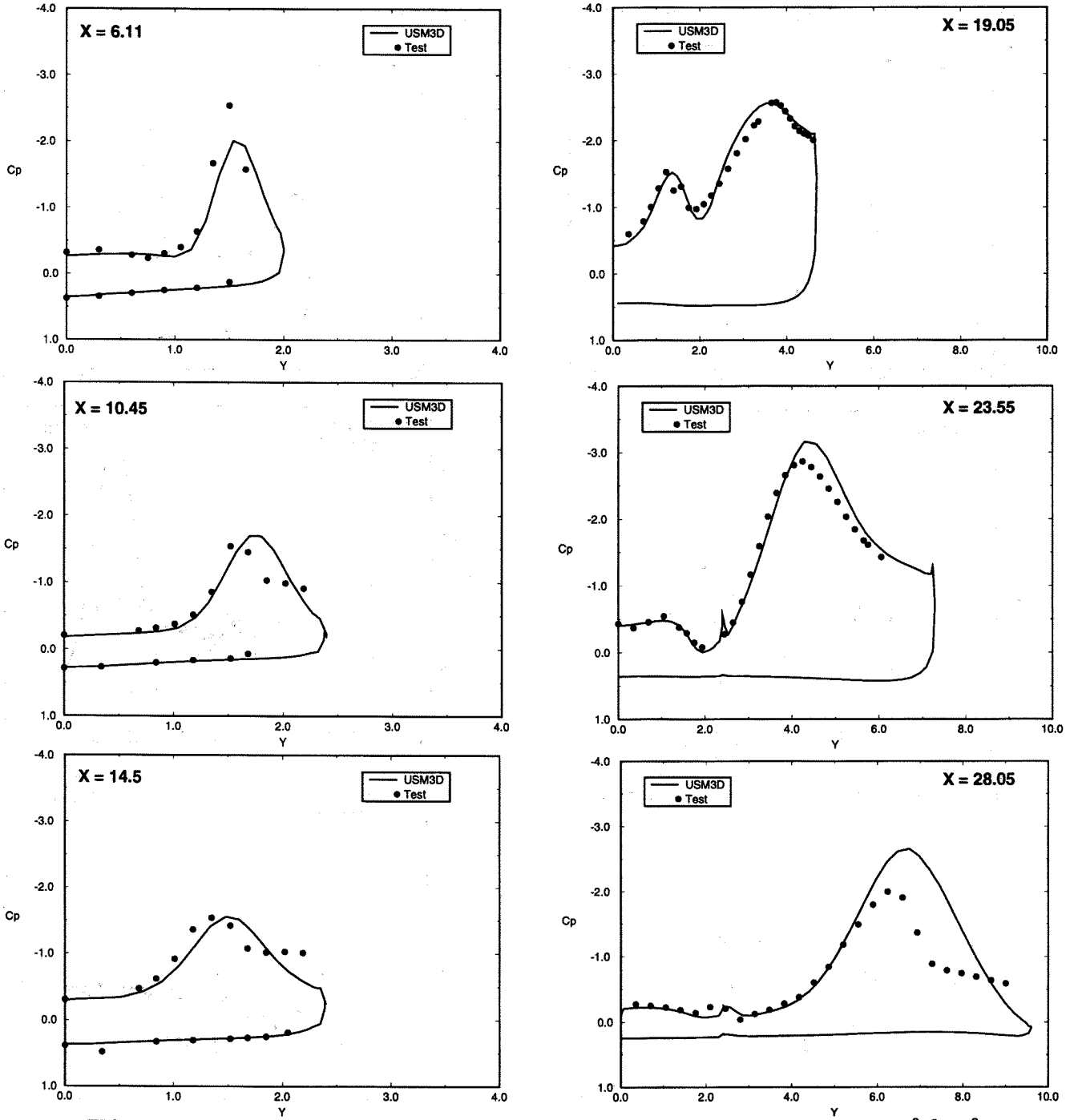

FIGURE 18 - Correlation of Computed and Measured Surface C_p, MTVI Model, M = 0.4, $\alpha = 25^o$, $\beta = 0^o$

the memory requirement must be aggressively pursued.

(3) The predicted trends of force and moment coefficient variation with angle of attack agreed fairly well with those from experiments. However, the lift coefficient reached a maximum at an angle of attack that was approximately 5° less than the measured value for all test cases. Further investigation is needed to identify the causes of this discrepancy. One possibility is that grid distribution was too sparse in the vortical-flow regions at angles of attack near maximum lift when the vortices moved farther away from the surface. The sparse grid with its large cell size might have introduced relatively large amounts of numerical dissipation contributing to premature vortex burst. Adding a solution-adaptive grid capability to the method is highly desirable. Also, the role of viscous effects needs to be studied using the RANS version under development.

The promise of the unstructured-grid CFD for vortical-flow simulation is clearly demonstrated by the results of the present study. With further enhancements in areas identified above, the unstructured-grid methods will provide a more effective means of generating aerodynamic data to support aircraft design needs as compared to the structured-grid methods presently in use.

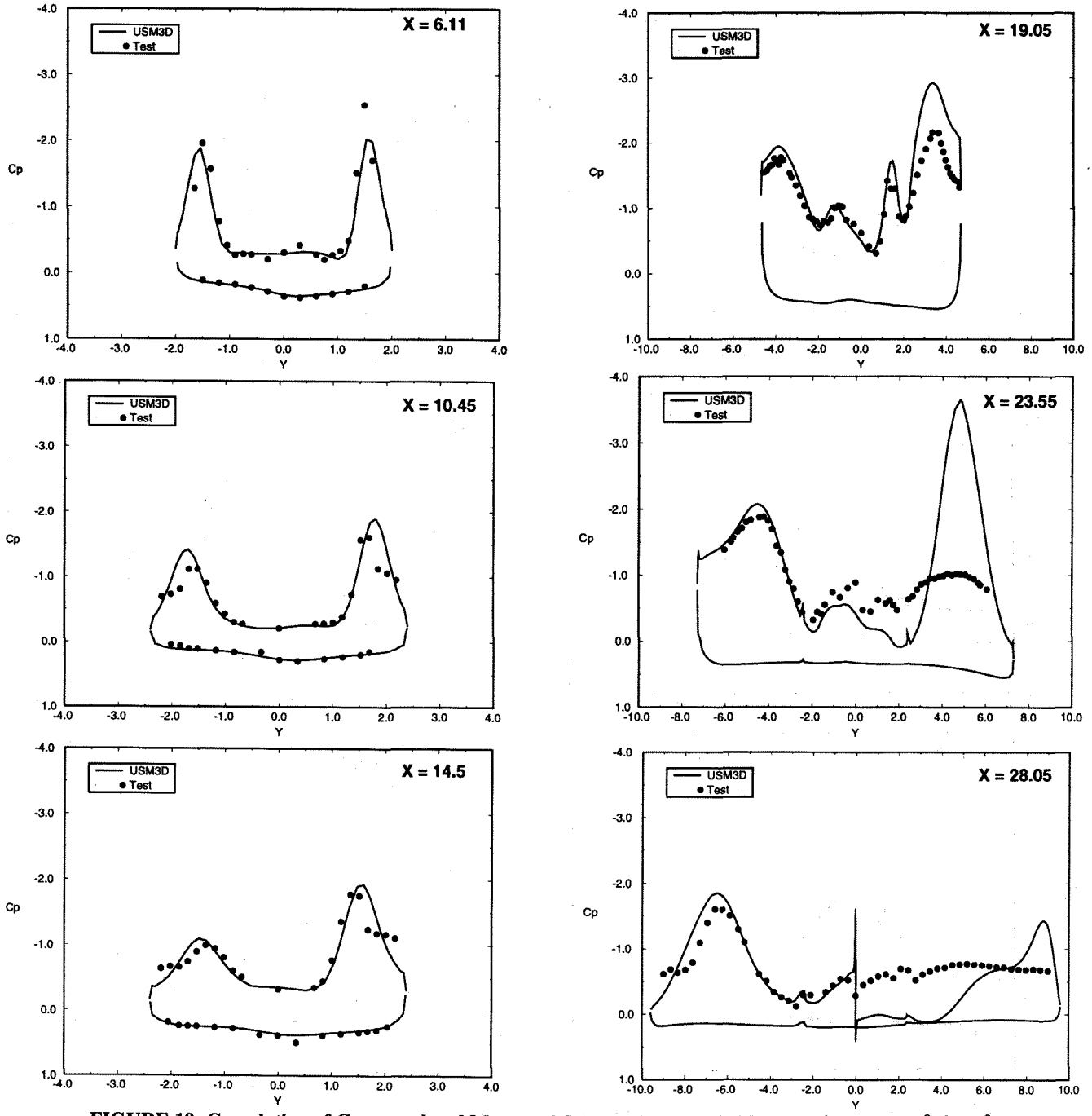

FIGURE 19- Correlation of Computed and Measured Surface C_p, MTVI Model, M = 0.4, $\alpha = 25^o$, $\beta = 4^o$

Acknowledgments

This paper was prepared under an Independent Research & Development project of the Lockheed Martin Aeronautical Systems, Marietta, Georgia. The MTVI analysis was sponsored by NASA-Langley Research Center, Hampton, Virginia, with Mr. F. Ghaffari as the technical monitor. The use of the Cray C-90 supercomputer at the NASA Numerical Aerodynamics Simulation (NAS) facility is gratefully acknowledged. Thanks are due to Dr. N.T. Frink of NASA-Langley for providing Version 4.3 of the USM3D flow solver and sharing his experiences with the authors.

References

1. Polhamus, E.C., "A Concept of the Vortex Lift of Sharp Edge Delta Wings Based on a Leading-Edge Suction Analogy," NASA TN D-3767, 1966.
2. Lamar, J.E. and Gloss, B.B., "Subsonic Aerodynamic Characteristics of Interacting Lifting Surfaces with Separated Flow Around Sharp Edges Predicted by a Vortex-Lattice Method," NASA TN D-7921, 1975.
3. Lan, C.E. and Chang, Jen-Fu, "Calculation of Vortex Lift Effect for Cambered Wings by suction Analogy," NASA CR 3449, 1981.
4. Luckring, J.M., Schoonover, W.E., and Frink, N.T., "Recent Advances in Applying Free Vortex Sheet Theory for the Estimation of Vortex Flow Aerodynamics," AIAA 82-0095, January 1982.
5. Raj, P., Keen, J.M. and Singer, S.W., "Applications of an Euler Aerodynamic Method to Free-Vortex Flow Simulation," *Journal of Aircraft*, Vol. 27, No. 11, 1990, pp. 941-949.
6. "Computational Aerodynamics Based on the Euler Equations," Sloof, J.W. and Schmidt, W., eds., Chapter 4.3, AGARD-AG-325, 1994, pp. 161-172.
7. Kinard, T.A., Harris, B.W., and Raj, P., "Computational Simulation of Benign and Burst Vortex Flows," AIAA 95-1815, June 1995.
8. Rizk, Y.M., Schiff, L.B., and Gee, K., "Numerical Prediction of the Unsteady Flowfield Around the F-18 Aircraft at Large Incidence," AIAA 91-0020, January 1991.
9. Ghaffari, F., "Navier-Stokes, Flight, and Wind Tunnel Flow Analysis for the F/A-18 Aircraft," NASA TP-3478, December 1994.
10. Dacles-Mariani, J., Zilliac, G.G., Chow, J.S., and Bradshaw, P., "Numerical/Experimental Study of a Wingtip Vortex in the Near Field," *AIAA Journal*, Vol. 33, No. 9, 1995, pp. 1561-1568.
11. Baker, T.J., "Prospects and Expectations for Unstructured Methods," NASA CP-3291, 1995, pp. 273-288.
12. Frink, N.T., Pirzadeh, S., and Parikh, P., "An Unstructured-Grid Software System for Solving Complex Aerodynamic Problems," NASA CP-3291, 1995, pp. 289-308.
13. Karman, Jr., S.L., "SPLITFLOW: A 3D Unstructured Cartesian/Prismatic Grid CFD Code for Complex Geometries," AIAA 95-0343, January 1995.
14. Melton, J.E., Berger, M.J., Aftosmis, M.J., and Wong, M.D., "Development and Application of a 3D Cartesian Grid Euler Method," NASA CP-3291, 1995, pp. 225-249.
15. Abolhassani, J., "GridTool: A Surface Modeling and Grid Generation Tool," NASA CP-3291, 1995, pp. 821-832.
16. "The Initial Graphics Exchange Specification (IGES) Version 5.0," National Computer Association, IGES/PDES Organization, 2722 Merrilee Drive, Suite 200, Fairfax, VA 22301.
17. Parikh, P., Pirzadeh, S., and Lohner, R., "A Package for 3-D Unstructured Grid Generation, Finite-Element flow Solution, and Flow-Field Visualization," NASA CR-182090, 1990.
18. Pirzadeh, S., "Structured Background Grids for Generation of Unstructured Grids by Advancing Front Method," AIAA 91-3233, January 1991.
19. Frink, N.T., "Upwind Scheme for Solving the Euler Equations on Unstructured Tetrahedral Meshes," *AIAA Journal*, Vol. 30, No. 1, 1992, pp. 70-77.
20. Frink, N.T., private communication.
21. Frink, N.T., "Recent Progress Toward a Three-Dimensional Unstructured Navier-Stokes Flow Solver," AIAA 94-0061, January 1994.
22. Turner, P.J., "ACE/gr User's Manual," Center for Coastal and Land-Margin Research, Oregon Graduate Institute of Science and Technology, Beaverton, OR 97006-1999, 1993.
23. Wentz, Jr., W.H., "Effects of Leading-edge Camber on Low-speed Characteristics of Slender Delta Wings," NASA CR-2002, 1972.
24. Wentz, Jr., W.H. and McMahon, M.C., "An Experimental Investigation of the Flow Fields About Delta and Double-Delta Wings at Low Speeds," NASA CR-521, 1966.
25. Kinard, T.A. and Raj, P., "An Euler Technology Assessment for Preliminary Design - Compressibility Predictions by Employing the Unstructured Grid USM3D Code," NASA CR 4711, March 1996.
26. Kinard, T.A., Finley, D.B., and Karman, Jr., S.L., "Prediction of Compressibility Effects Using Unstructured Euler Analysis on Vortex Dominated Flow Fields," AIAA 96-2499, June 1996.